

# **TEMPERATURE EFFECTS ON THE EMISSION PROPERTIES OF Yb-DOPED FIBERS (Postprint)**

**T.C. Newell  
P. Peterson  
A. Gavrielides  
M.P. Sharma**

**29 November 2006**

**Journal Article**

**APPROVED FOR PUBLIC RELEASE; DISTRIBUTION IS UNLIMITED.**



**AIR FORCE RESEARCH LABORATORY  
Directed Energy Directorate  
3550 Aberdeen Ave SE  
AIR FORCE MATERIEL COMMAND  
KIRTLAND AIR FORCE BASE, NM 87117-5776**

| <b>REPORT DOCUMENTATION PAGE</b>  |                                    |  |  | <i>Form Approved</i><br><i>OMB No. 0704-0188</i>                         |  |
|---|------------------------------------|--|--|--|--|
| Public reporting burden for this collection of information is estimated to average 1 hour per response, including the time for reviewing instructions, searching existing data sources, gathering and maintaining the data needed, and completing and reviewing this collection of information. Send comments regarding this burden estimate or any other aspect of this collection of information, including suggestions for reducing this burden to Department of Defense, Washington Headquarters Services, Directorate for Information Operations and Reports (0704-0188), 1215 Jefferson Davis Highway, Suite 1204, Arlington, VA 22202-4302. Respondents should be aware that notwithstanding any other provision of law, no person shall be subject to any penalty for failing to comply with a collection of information if it does not display a currently valid OMB control number. <b>PLEASE DO NOT RETURN YOUR FORM TO THE ABOVE ADDRESS.</b> |                                    |  |  |  |  |
| <b>1. REPORT DATE (DD-MM-YYYY)</b><br>29-11-2006  |                                    | <b>2. REPORT TYPE</b><br>Journal Article |  | <b>3. DATES COVERED (From - To)</b><br>01-10-04 - 01-06-06               |  |
| <b>4. TITLE AND SUBTITLE</b><br>TEMPERATURE EFFECTS ON THE EMISSION PROPERTIES OF<br>Yb-DOPED FIBER (Postprint)   |                                    |  |  | <b>5a. CONTRACT NUMBER</b><br>In House (DF297206)                        |  |
|   |                                    |  |  | <b>5b. GRANT NUMBER</b><br>N/A   |  |
|   |                                    |  |  | <b>5c. PROGRAM ELEMENT NUMBER</b><br>61102F                              |  |
| <b>6. AUTHOR(S)</b><br>T.C. Newell, P. Peterson, A. Gavrielides, M.P. Sharma*   |                                    |  |  | <b>5d. PROJECT NUMBER</b><br>2301  |  |
|   |                                    |  |  | <b>5e. TASK NUMBER</b><br>LR   |  |
|   |                                    |  |  | <b>5f. WORK UNIT NUMBER</b><br>02  |  |
| <b>7. PERFORMING ORGANIZATION NAME(S) AND ADDRESS(ES)</b><br><br>Air Force Research Laboratory      *University of New Mexico<br>3550 Aberdeen Ave SE              Physics Department<br>Kirtland AFB, NM 87117-5776      800 Yale Blvd NE<br>Albuquerque, NM 87131   |                                    |  |  | <b>8. PERFORMING ORGANIZATION REPORT</b>                                 |  |
| <b>9. SPONSORING / MONITORING AGENCY NAME(S) AND ADDRESS(ES)</b><br>Air Force Research Laboratory<br>3550 Aberdeen Ave SE<br>Kirtland AFB, NM 87117-5776  |                                    |  |  | <b>10. SPONSOR/MONITOR'S ACRONYM(S)</b><br>DELO                          |  |
|   |                                    |  |  | <b>11. SPONSOR/MONITOR'S REPORT NUMBER(S)</b><br>AFRL-DE-PS-JA-2007-1005 |  |
| <b>12. DISTRIBUTION / AVAILABILITY STATEMENT</b><br><br>APPROVED FOR PUBLIC RELEASE; DISTRIBUTION IS UNLIMITED.   |                                    |  |  |  |  |
| <b>13. SUPPLEMENTARY NOTES</b><br>Submitted for publication in Optics Communications, <b>273</b> , Issue 1, pp. 256-259, 1 May 2007 <b>GOVERNMENT PURPOSE RIGHTS</b>  |                                    |  |  |  |  |
| <b>14. ABSRACT</b><br>Ytterbium-doped fiber lasers are making impressive leaps in power production. Yet in spite of fibers large surface area to volume ratio which is beneficial for cooling, such power inevitably leads to high core temperatures that in turn affect the laser performance. In this letter, the temperature effects on the emission and fluorescence lifetime of ytterbium doped optical fibers are investigated. From these the temperature dependent emission and absorption cross sections are calculated. A corresponding theoretical treatment presents the necessary conditions to eliminate radiation trapping.  |                                    |  |  |  |  |
| <b>15. SUBJECT TERMS</b><br>Lasers, temperature, emission   |                                    |  |  |  |  |
| <b>16. SECURITY CLASSIFICATION OF:</b><br>UNCLASSIFIED  |                                    |  | <b>17. LIMITATION OF ABSTRACT</b><br><br>SAR | <b>18. NUMBER OF PAGES</b><br><br>9                                      | <b>19a. NAME OF RESPONSIBLE PERSON</b><br>Phillip Peterson       |
| <b>a. REPORT</b><br>UNCLASSIFIED  | <b>b. ABSTRACT</b><br>UNCLASSIFIED | <b>c. THIS PAGE</b><br>UNCLASSIFIED      |  |  | <b>19b. TELEPHONE NUMBER (include area code)</b><br>505-846-9301 |

# Temperature Effects on the Emission Properties of Yb-doped optical fibers.

T. C. Newell, P. Peterson, and A. Gavrielides

*Directed Energy Directorate, 3550 Aberdeen Ave. Kirtland AFB NM 87117*

M. P. Sharma

*Physics Department, 800 Yale Blvd NE, University of New Mexico, Albuquerque, NM 87131*

**Abstract:** Ytterbium-doped fiber lasers are making impressive leaps in power production. Yet in spite of fibers large surface area to volume ratio which is beneficial for cooling, such power inevitably leads to high core temperatures that in turn affect the laser performance. In this letter, the temperature effects on the emission and fluorescence lifetime of ytterbium doped optical fibers are investigated. From these the temperature dependent emission and absorption cross sections are calculated. A corresponding theoretical treatment presents the necessary conditions to eliminate radiation trapping.

©2006 Optical Society of America

**OCIS codes:** (060.2270) Fiber characterization; (060.2290) Fiber materials; (160.5690) Rare earth doped materials; (300.2140) Emission

---

## References and Links

1. S. Z. Zhao, A. Rapaport, J. Dong, B. Chen, P. Z. Deng, and M. Bass, "Temperature dependence of the 1.03  $\mu\text{m}$  stimulated emission cross section of Cr:Yb:YAG crystal," *Opt. Mat.* **27**, 1329-1332 (2005).
2. S. Sumida and T. Y. Fan, "Emission spectra and fluorescence lifetime measurements of Yb:YAG as a function of temperature," *OSA Proc. Adv. Solid State Lasers* **20**, 100-102, (1994).
3. T. Sun, Z.Y. Zhang, K.T.V. Grattan, and A. W. Palmer, "Ytterbium-based fluorescence decay time fiber optic temperature sensor systems," *Rev. Sci. Instrum.* **69**, 4179-4185 (1998).
4. E. Maurice, S.A. Wade, S.F. Collins, G. Monnom and G.W. Baxter, "Self-referenced point temperature sensor based on a fluorescence intensity ratio in Yb<sup>3+</sup>-doped silica fiber," *Appl. Opt.* **36**, 8264-8269 (1997).
5. D.A. Gruk, A. S. Kurkov, V. M. Paramonov, and E. M. Dianov, "Effect of heating on the optical properties of Yb<sup>3+</sup> -doped fibres and fibre lasers," *Quantum Electron.*, **34**, 579-582 (2004).
6. H. M. Pask, R. J. Carman, D.C. Hanna, A.C. Tropper, C.J. Mackechnie, P. R. Barber, and J. M. Dawes, "Ytterbium-doped silica fiber lasers: versatile sources for the 1-1.2  $\mu\text{m}$  region," *IEEE Select. Topics Quantum. Electron.* **1**, 2-13 (1995).
7. J. Y. Allain, M. Monerie, H. Poignant, "Ytterbium-doped fluoride fibre laser operating at 1.02  $\mu\text{m}$ ," *Electron. Lett.* **28**, 988-9 (1992).
8. D.C. Hanna, R. M. Percival, I. R. Perry, R. G. Smart, P.J. Suni, A.C. Tropper, "An ytterbium-doped monomode fibre laser: broadly tunable operation from 1.010  $\mu\text{m}$  to 1.162  $\mu\text{m}$  and three-level operation at 974 nm," *J. Mod. Opt.* **37**, 517-25 (1990).
9. Z. Zhang, K.T.V. Grattan, and A.W. Palmer, "Thermal characteristics of alexandrite fluorescence decay at high temperatures, induced by a visible laser diode emission," *J. Appl. Phys.* **73**, 3493-3498 (1993).
10. E. McCumber, "Theory of phonon-terminated optical masers," *Phys. Rev.* **134**, A299-A306 (1964).
11. F. Moulton, "Spectroscopic and laser characteristics of Ti:Al<sub>2</sub>O<sub>3</sub>," *J. Opt. Soc. Am. B* **3**, 125-133 (1986).
12. S. R. Bowman, S. P. O'Connor, and S. Biswal, "Ytterbium laser with reduced thermal loading," *IEEE J. Quantum Electron.* **41**, 1510-1517 (2005).
13. S. Dai, A. Sugiyama, L. Hu, S. Liu, G. Huand, and Z. Jiang, "The spectrum and laser properties of ytterbium doped phosphate glass at low temperatures," *J. of Non-Crystalline Solids*, 311, 138-144(2002).

---

## I. Introduction

When ytterbium (Yb) is seeded in the amorphous silica glass core of an optical fiber, the emission and absorption spectrum due to the subbands of the two manifolds,  $^2F_{5/2}$  and  $^2F_{7/2}$ , broaden beyond that which would be found in a crystalline structure like YAG [1]. While there is a large interest in cryogenic Yb:YAG lasers [2], with exception to fiber temperature sensors [3, 4] less research exists for Yb:silica. Such temperature effects have generally not been of much concern although Gruk [5] observed that improved long wavelength lasing can be obtained at high

temperatures. Furthermore, now that demonstrated CW laser powers have exceeded 2 kW very high core temperatures may be reached. Here heating inevitably occurs in spite of the fibers large surface area to volume ratio.

Compared to other rare-earth ions, Yb possesses a remarkably simple atomic structure. With only two principle levels that are separated by some  $8750\text{ cm}^{-1}$ , it is the most ideal rare-earth element for lasing. Weak multi-phonon decay is practically the only non-radiative channel that exists. Fig. 1 shows our energy level diagram for Yb with a silica core. This diagram is inferred from our low temperature measurements which we discuss in the following sections. The three lines of the upper  $^2F_{5/2}$  manifold are denoted a, b, and c. The four lines of the lower  $^2F_{7/2}$  manifold are labeled i, j, k, and l. Included in this diagram are arrows indicating absorption lines at 977nm, 960nm, 920nm, and emission lines at 977nm, 1020nm, 1032nm, 1069nm. The latter four lines originate from level (a) in the upper manifold as can be seen from the low temperature emission spectra shown in fig. (3). Note that this places the 4 lower levels (i, j, k, l) at  $425\text{ cm}^{-1}$ ,  $530\text{ cm}^{-1}$ ,  $865\text{ cm}^{-1}$  and  $1129\text{ cm}^{-1}$ , respectively. Additionally, although we do not show it, the absorption cross section derived via the McCumber formula show an absorption line at 960nm. This then verifies the existence of the (j) level at  $425\text{ cm}^{-1}$ . The other lower levels are in the neighborhood of previous measurements [6-8]. The apparent discrepancy between these references is resolved by realizing that the energy spacing depends on the constituent elements in the fiber core. Also broadening of the levels renders it difficult to establish their true values. Emission data obtained at cryogenic temperatures reveals the dominant energy transitions, and in particular, an energy level at  $425\text{ cm}^{-1}$ . Additionally, the energy spacing between level a and b can be verified by curve-fitting to fluorescence lifetime data, as we show in section 2.2.

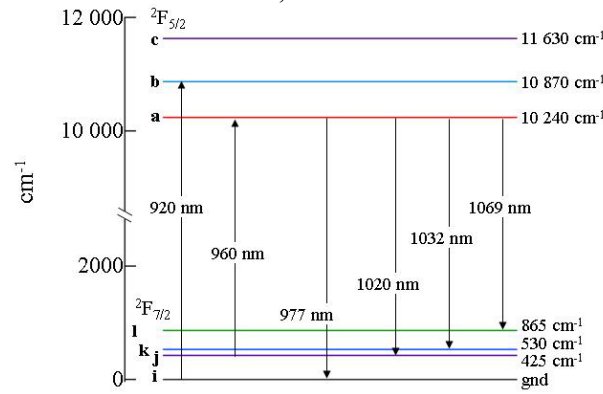


Figure 1. Energy levels of Ytterbium:Silica.

Lasing typically occurs from 1030 nm to beyond 1150 nm. Although the laser is considered as being quasi 3-level, it is more of a 4-level system at cryogenic temperatures when the thermally induced broadening of the levels is minimized and when the thermal equilibrium distribution of electrons render them frozen in the ground state. It also should behave more like a 4-level system for very long lasing wavelengths when the state into which the electron falls is well above the ground state.

In this work a 910 nm diode laser pumps the doped fiber. Consequently level c is not pumped. This is more representative of typical fiber laser pumping schemes, and furthermore the system can be modeled using only the two upper levels [9]. In section II the experiments are described from which the fluorescence lifetime and spontaneous emission are obtained. The emission cross-section is then computed from the results. In section III we present a brief analysis of the radiation trapping conditions. Conclusions are summarized in section IV.

## II. Experimental Investigations

### 2.1 Experimental Arrangement

The fiber used is commercially available dual-clad Yb-doped fiber manufactured by OFS (part #Comcode 107 986 820). The  $6\text{ }\mu\text{m}$  diameter silica core is Yb-doped. A  $210\text{ }\mu\text{m}$  diameter silica cladding follows, and the outer polymer jacket is  $300\text{ }\mu\text{m}$ . A  $0.65\text{ mm}$  section of the doped fiber is fusion spliced to one arm of a single mode 2x2 coupler. The end is angle cleaved to suppress back reflections, and it is short to minimize any amplified spontaneous emission and radiative trapping. Should radiative trapping occur, one observes a decrease in the ratio of the spontaneous emission peak at 977 nm to the peak at 1050 nm and an increase in the fluorescence lifetime, see section III. For a cryogenic measurement, the doped fiber section is bathed in liquid nitrogen cryostat. For high temperature

measurements, it is placed within a custom built oven. The doped fiber is pumped with a low frequency sinusoidally modulated 910 nm diode laser. The spontaneous emission propagating counter to the direction of the pump is input into a Spectral Products DK480 monochromator and detected by a New Focus femtowatt photodetector. Prior to the experiments the detector was spectrally calibrated using a white light source and calibrated integrating sphere. The resulting voltage signal is measured with a Stanford Research Systems lock-in amplifier that is frequency locked to the laser diode modulation frequency. Stray pump light is blocked using a 950 nm long wave pass filter. A computer controls the acquisition process.

The setup for a fluorescence lifetime measurement uses the same coupler and fiber, but the fiber is pumped with a pulsed source at a low duty cycle. Backward propagating light from the Yb-fiber was filtered with a 950 nm long wave pass filter to remove the pump and coupled to a high gain high bandwidth detector. The ensuing signal was captured by an oscilloscope operating in a signal averaging mode.

## 2.2 Fluorescence Lifetime

Measurements were made between temperatures from 77 K to 443 K. Near 77 K, the observed lifetime is 0.885 ms. At 443 K, the lifetime decreases 59  $\mu$ s to 0.826 ms. The fluorescence lifetime as a function of temperature is shown in Fig. 2. The error bars are 2 standard deviations above and below the average as determined by a linear curve fit to the log of the decay data. The dotted line through the data points is a curve fit from a two-level model [9]. By considering the decay from the lower two thermalized levels of the  $^2F_{5/2}$  manifold to the ground state of the  $^2F_{7/2}$  manifold, the lifetime can be modeled by  $\tau = (1 + e^{-\Delta E/kT}) / (1/\tau_a + 1/\tau_b e^{-\Delta E/kT})$ . Here  $\tau_a$  is the lifetime of the lowest level, a, and  $\tau_b$  is that of level b.  $\Delta E$  is the energy separation between the two states. When this function is fit to our data the energy separation between the lowest two  $^2F_{7/2}$  levels is 630  $\text{cm}^{-1}$ . This value matches that which is obtained from observing the emission peaks seen in Fig. 3. We find that  $\tau_a = 0.884$  ms and  $\tau_b = 0.547$  ms. In fibers that have been subjected to very high temperatures, the lifetime has been observed to decrease very rapidly beyond activation energy [3]. We did not operate the fiber at high enough temperatures to observe this quenching effect.

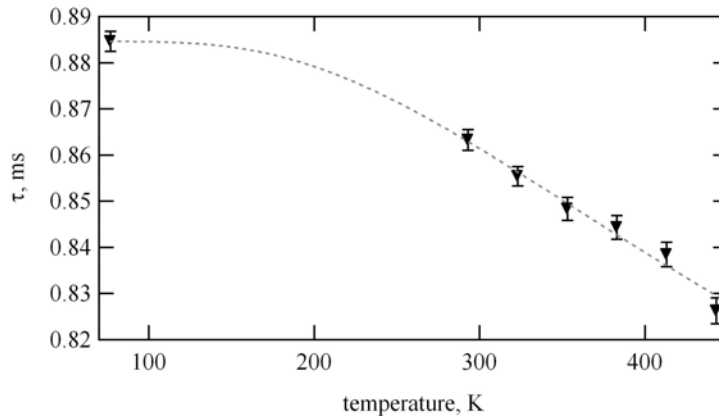


Figure 2. The fluorescence lifetime as a function of temperature. The dotted line traces a curve fit using a two-level model.

## 2.3 Spontaneous Emission.

Spontaneous emission was measured at temperatures of 77 K, 293 K (20°C), 323 K (50°C), 383 K (110°C), and 443 K (140°C). The emission data is shown in Fig. 3. The 77 K spectra shows emission at 1020 nm, 1032 nm, and 1069 nm. These lines show that there are levels at 425  $\text{cm}^{-1}$ , 530  $\text{cm}^{-1}$ , and 865  $\text{cm}^{-1}$  above the ground state (i). This is the first time, as far as we know, that a level near 425  $\text{cm}^{-1}$  has been identified in Yb silica, although measurements in low temperature Yb phosphates indicate this same level [13]. At high temperatures the 1019 nm plateau and 1032 nm peak coalesce into a smooth broad rise, which is due to the broadening of the states, particularly level a. The 977 nm peak decreases substantially due in part to broadening around the shoulders. And as the thermalization of electrons populates the  $^2F_{5/2}$  manifold's higher energy levels, absorption of the 910 nm photon decreases.

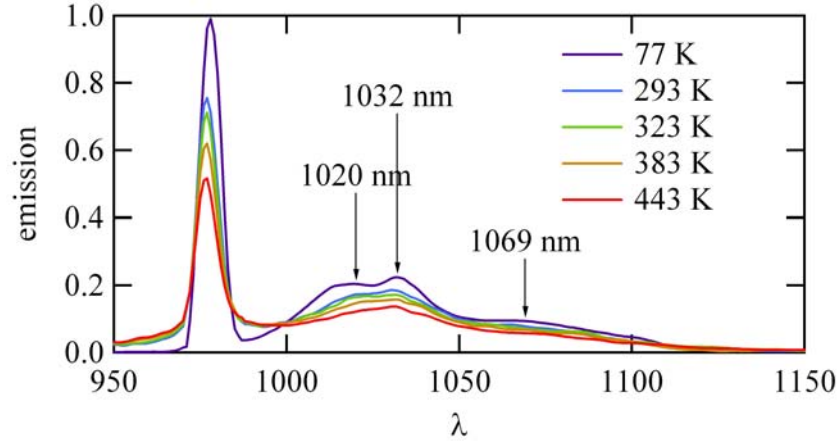


Figure 3. Spontaneous emission spectra for temperatures ranging from 77 K to 443 K.

#### 2.4 Gain Cross-section.

Using the work of McCumber [10], Moulton [11] derives the relationship between the measured emission spectra  $s(\lambda)$ , seen in Fig. (3), and the emission cross-section. They find that  $\sigma(\lambda) = \lambda^5 (8\pi c n^2 \tau)^{-1} s(\lambda) \langle \lambda \rangle^{-1}$  where  $\langle \lambda \rangle$  is the integral of the product  $\lambda s(\lambda)$ , and  $\sigma(\lambda)$  is the emission cross-section. In the section III we derive this equation through the emission field and inversion equation to find the radiation trapping limits. This equation applied to the data in Fig. (3) yields Fig. (4) for the emission cross-section at temperatures of 77 K, 293 K, 323 K, 383 K, and 443 K. Again, in Fig(4) we see the 4 dominate emission lines at 978nm, 1020 nm, 1032 nm, and 1069 nm at the low temperature of 77 K. While it is clear that an increase in emission at low temperatures should lead to a greater emission cross-section, the expected benefit is not realized in its entirety since the emission lifetime is also increasing. In fact, beyond 1035 nm, the data shows very little change in cross-section with temperature. As the absorption decreases with increasing wavelength, the net gain portends excellent high temperature performance at long wavelengths. Indeed, this has been observed in Ref. [5].The

McCumber formula [10] applied to the data in Fig. (4) generates the absorption cross-section shown in Fig. (5). The low temperature cross section shows a weak but discernable absorption peak near 960nm which grows as the temperature increases. This corresponds to the (j-b) transition and again establishes the  $\Delta E_{j,i} = 425 \text{ cm}^{-1}$  and the  $\Delta E_{b,a} = 630 \text{ cm}^{-1}$  levels. We note that in generating the absorption spectra the zero photon line is shifted by about 1% between 77 K and 443 K.

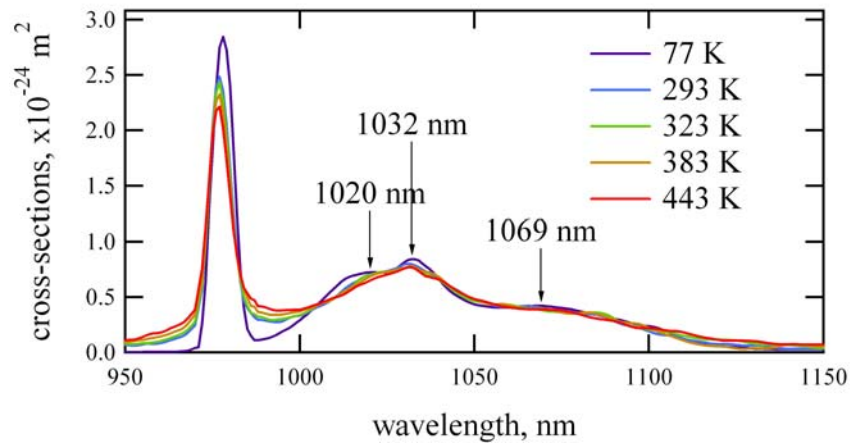


Figure 4. Gain cross-section computed using the measured fluorescence lifetime and spontaneous emission data.

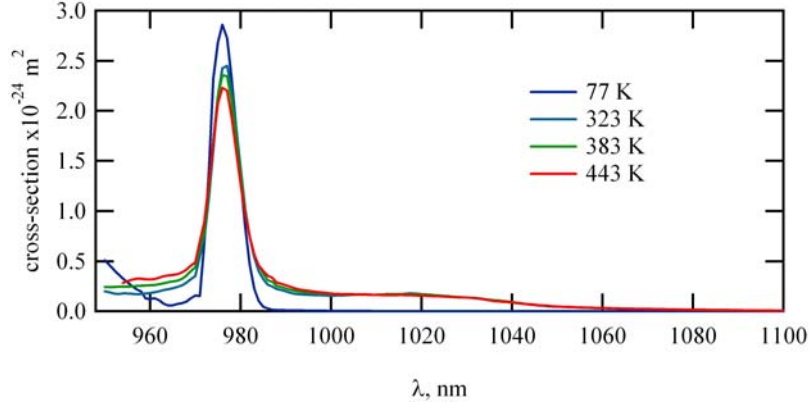


Figure 5. The absorption cross-section computed using experimentally measured emission data along with the McCumber transform.

### 3.1 Radiation Trapping Conditions

The radiative decay time and the emission and absorption cross section can be altered by cavity effects, fluorescence absorption, and temperature dependent pumping efficiency. In the following we briefly discuss the effects of these three processes on the decay time and cross section measurements.

Of these two measurements we begin with the decay time. We assume that the inversion and intensities are described in the mean field approximation (MFA). Thus, the rate equation for the upper level population in Yb takes the well known form Ref. [12]

$$\frac{dN_2}{dt} = \frac{I_p \sigma_a(\lambda_p, T)}{h\nu_p} \left( N_0 - \frac{N_2}{\beta(\lambda_p, T)} \right) - \frac{N_2}{\tau_r} + \left\langle \frac{I_F \sigma_a(\lambda, T)}{h\nu} \left( N_0 - \frac{N_2}{\beta(\lambda, T)} \right) \right\rangle. \quad (1) \text{ where we have ignored a}$$

lasing term. The pumping intensity  $I_p$  is at a wavelength of  $\lambda_p$  and the fluorescence intensity is related to the spectral intensity by  $I_F = \int I_F(\lambda) d\lambda$ . The upper state relaxation decay time is  $\tau_r$ . Also,  $\beta(\lambda, T) = \sigma_a(\lambda, T) / [(\sigma_a(\lambda, T) + \sigma_e(\lambda, T))]$  where the subscripts indicate fluorescence absorption and emission. The temperature dependence of these is connected through the McCumber relation; also, we emphasize the temperature dependence as an explicit variable. We assume that the fluorescence radiation fills the entire core and the amount which escapes the end is determined by  $\Omega/4\pi$  where  $\Omega$  is the solid angle.

Again, using the MFA the upper state population is coupled to the fluorescence spectral intensity  $I_F(\lambda, T)$  by

$$\frac{dI_F(\lambda, T)}{dt} = -\frac{I_F(\lambda, T)}{\tau_p} + \frac{\Omega}{4\pi} \frac{c}{n(\lambda)} \frac{h\nu}{\tau_r} \frac{g(\lambda, T)}{\int g(\lambda, T) d\lambda} N_2. \quad (2) \quad \text{Here the time } \tau_p$$

incorporates the contributions from the cavity decay time,  $\tau_c$ , and the absorption rate of the fluorescing field as

$$\frac{1}{\tau_p} = \frac{1}{\tau_c} + c \left( N_0 - \frac{N_2}{\beta(\lambda, T)} \right) \sigma_a(\lambda, T), \quad \tau_c = \frac{2nL/c}{1 - R_1 R_2}. \quad (3) \text{ where } R_1, R_2 \text{ are the}$$

cavity reflectivities, and  $L$  is the cavity length. Furthermore, the line shape  $g(\lambda, T)$  is related to the emission cross section by

$$g(\lambda) = \frac{8\pi n^2(\lambda) c \tau_r \sigma_e(\lambda)}{\lambda^4}, \quad (4) \text{ where the index of}$$

refraction is, of course,  $n(\lambda)$ .

Our experiment, as well as that of others, shows that  $I_F(\lambda)$  decays on the time scale of  $\tau_r$ ; thus,  $1/\tau_r \ll 1/\tau_c$  since our cavity length is 0.6 mm. Consequently, the solution to the spectral intensity equation collapses to

$$I_F(\lambda, T) = \tau_p \frac{\Omega}{4\pi} \frac{c}{n} \frac{h\nu}{\tau_r} \frac{g(\lambda, T)}{\int g(\lambda, T) d\lambda} N_2, \quad (5)$$

where  $\tau_p$  can be rewritten as

$$\tau_p = \frac{\tau_c}{1 + \tau_c \alpha(\lambda, T) \frac{c}{n(\lambda)}}, \quad (6)$$

and  $\alpha(\lambda, T) = \sigma_a(\lambda, T)(N_0 - N_2/\beta(\lambda, T))$ . Inserting these into the upper state population rate equation gives

$$\begin{aligned} \frac{dN_2}{dt} = & \frac{I_p \sigma_a(\lambda_p, T)}{h\nu_p} \left( N_0 - \frac{N_2}{\beta(\lambda_p, T)} \right) - \frac{N_2}{\tau_r} + \frac{\Omega}{4\pi} \frac{c}{n} \frac{\tau_c}{\tau_r} \times \\ & \left\langle \frac{\sigma_a(\lambda, T)}{1 + \tau_c \sigma_a(\lambda, T)(N_0 - N_2/\beta(\lambda, T)) \frac{c}{n}} \frac{g(\lambda, T)}{\int g(\lambda, T) d\lambda} N_2 \left( N_0 - \frac{N_2}{\beta(\lambda, T)} \right) \right\rangle. \end{aligned} \quad (7)$$

However, if  $N_0 \gg N_2/\beta(\lambda, T)$  then the upper level population equation takes the form

$$\frac{dN_2}{dt} = \frac{I_p \sigma_a(\lambda_p, T)}{h\nu_p} N_0 - \frac{N_2}{\tau_{eff}}, \quad (8)$$

where

$$\frac{1}{\tau_{eff}} = \frac{1}{\tau_r} \left( 1 - \frac{c}{n} \tau_c N_0 \left\langle \frac{\sigma_a(\lambda, T)}{1 + \tau_c \sigma_a(\lambda, T) N_0 c/n} \frac{g(\lambda, T)}{\int g(\lambda, T) d\lambda} \right\rangle \right). \quad (9)$$

Thus, the effect of radiation trapping, either in the form of the cavity reflectivity or absorption, is to decrease the decay rate. Moreover, if  $\tau_c \sigma_a(\lambda, T) N_0 c/n \ll 1$  then we are left with  $\tau_{eff} \approx \tau_r$ . In passing we note that the lifetime measured in reference [13] does increase with temperature. The authors [13] conclude that radiation trapping is present in their experiment due to the high doping levels. After inserting their numbers in Eq. (9) we find that the lifetime is increased by about a factor of 2; this is consistent with their measurements. Next we turn to the consideration of the cross sections by measuring the fluorescence in the reverse direction. We show how emission cross section is related to the fluorescing spectral intensity and the temperature dependent pumping. This process is entirely steady state so we start with

$$\frac{dI_{F\pm}}{dz} = \pm G(\lambda, T) I_{F\pm} \pm B(\lambda, T) \quad (10)$$

where

$$G(\lambda, T) = \sigma_a(\lambda, T) \left( N_0 - \frac{N_2(z)}{\beta(\lambda, T)} \right), \quad B(\lambda, T) = \frac{\Omega}{4\pi} \frac{h\nu}{\tau_r} \frac{g(\lambda)}{\int g(\lambda) d\lambda} N_2(z). \quad (11)$$

where  $I_F(T) = \int I_F(\lambda, T) d\lambda$ . These equations can be solved under very achievable experimental conditions. Our assumptions are:  $N_0 \gg N_2(z)/\beta(\lambda)$ ; and  $R_1, R_2$  are small so that the pump is undepleted, and consequently the forward and reverse fields are decoupled. Incorporating these assumptions, we have

$$F_R = \frac{B(\lambda, T)}{G(\lambda, T)} (1 - R_1) \frac{(R_2 \exp(G(\lambda, T)L) + 1)(\exp(G(\lambda, T)L) - 1)}{1 - R_1 R_2 \exp(2G(\lambda, T)L)}. \quad (12)$$

Further, if  $2G((\lambda, T)L) \ll 1$  and one facet is cleaved we obtain the simple form

$$F_R = (1 - R_1) B(\lambda, T) L = (1 - R_1) L \frac{\Omega}{4\pi} \frac{h\nu}{\tau_r} \frac{g(\lambda)}{\int g(\lambda) d\lambda} N_2. \quad (13)$$

Furthermore, with the above assumptions the upper state population approximates to

$$N_2 \approx \frac{\frac{N_0(I_P\sigma_a(\lambda_P,T))}{h\nu_P}}{\frac{I_P\sigma_a(\lambda_P,T)}{h\nu_P} + \frac{1}{\tau_r}}. \quad (14)$$

Here one can clearly see the temperature dependence of the pump absorption. By employing eq. (4) the measured spectral intensity can be cast into a form which includes the emission cross section as

$$F_R(\lambda, T) = K \frac{\Omega}{4\pi} \frac{hc}{\lambda} 8\pi n^2 c \frac{\sigma_e(\lambda)}{\lambda^4} \frac{N_2}{\int g(\lambda) d\lambda} \frac{c}{n}, \quad (15)$$

where  $K$  is a constant associated with the measurement process. Following the standard procedure of introducing the average wavelength  $\langle \lambda \rangle = \int \lambda F_R(\lambda) d\lambda$ , the cross section can be derived from the measured spectral intensity as

$$\sigma(\lambda) = \frac{\lambda^5 F_R(\lambda)}{8\pi n^2 c \tau_r \langle \lambda \rangle} \quad (16)$$

which is related to the absorption cross section through the McCumber equation. Thus, in the above approximations the temperature dependence of the pump absorption in Eq. (16) does not appear since it is wrapped up in the introduction of the average wavelength, derived from the measured  $F_R(\lambda)$ , and it effectively cancels.

However, in the more general case if the absorption of the radiation is not small then

$$F_R = \frac{B(\lambda, T)}{G(\lambda, T)} (1 - R_l) (\exp(G(\lambda, T)L) - 1) \quad (17)$$

which is coupled to the upper state population equation through eq. (14) and the cross section cannot be extracted in a simple manner.

#### IV. Summary

In this paper we use temperature as an investigative tool to determine spectroscopic characteristics of moderately doped Yb:silica fiber. Spontaneous emission and fluorescence lifetime measurements are used to calculate the emission cross-section as a function of temperature and to provide insight into the evolution of the emission lineshape. Cryogenic emission measurements yield insights into the lower  $^2F_{7/2}$  manifold. While fluorescence lifetime studies indicate the energy split between the lower two levels of the upper  $^2F_{5/2}$  manifold.

At the cryogenic temperatures we were able to reach, a substantial amount of homogenous and inhomogeneous broadening mechanisms remain. Still observed peaks in the spontaneous emission spectrum at 1020 nm, 1032 nm and 1069 nm in the emission indicate the energy levels of the lower  $^2F_{7/2}$  manifold. As for the fluorescence lifetime, when the temperature increases from 77K to 443K a small decrease of 8%, or roughly, 0.00013ms/K occurs. This decrease can be successfully explained by emission from a thermalized two upper level model with levels separated by  $630 \text{ cm}^{-1}$ . Absorption spectra not presented here also confirmed this separation.

At high temperatures, the evolution of the cross-section shows that temperature insensitive lasing should occur for longer wavelengths than the typical 1050-1080 nm wavelengths demonstrated. There are a number of applications where such qualities are highly desirable, and such a laser is the focus of future work.